Contrib Mineral Petrol (2003) 145: 61–74
DOI 10.1007/s00410-002-0432-z

ORIGINAL PAPER

Martin J. Whitehouse · John P. Platt

Dating high-grade metamorphism—constraints from rare-earth elements in zircon and garnet

Received: 22 February 2002 / Accepted: 31 October 2002 / Published online: 14 January 2003

Abstract We integrate petrography and SIMS REE analyses of garnet and polyphase zircon from a pelitic granulite adjacent to the Ronda peridotite, Betic Cordillera, southern Spain to constrain the significance of zircon U–Pb geochronology. Sillimanite inclusions in garnet rims suggest that they grew during decompression, and Ca enrichment in their rims records initiation of partial melting. Chondrite-normalised REE profiles of zircon cores are typically magmatic (positive La to Lu slope and Ce anomaly), whereas overgrowths have flat or negatively sloping heavy-REE profiles (Gd–Lu). The presence of rimmed zircon grains only in the garnet rims and the matrix suggests that this zircon phase grew after garnet had already sequestered heavy REEs, a process documented here by progressive depletion of heavy REE in the garnets from centre to rim. Combined with the textural evidence, we suggest that the U–Pb age of 21.3 ± 0.3 Ma obtained from the zircon rims dates a point on this decompression path rather than the peak metamorphic pressure.

Introduction

Zircon is the most commonly used mineral for U–Pb geochronology, primarily because of its remarkable chemical and mechanical stability during geological events, as well as its ability to grow or recrystallise under a wide range of conditions from igneous to metamorphic. Despite recent advances in analytical methods, the interpretation of ages may remain ambiguous, particularly in metamorphic rocks where the goal is to accurately relate pressure–temperature evolution to geochronology. The common assumption that metamorphic zircon growth corresponds to the temperature peak (T_{max}) and, by extension, the pressure peak (P_{max}) may be seriously in error, especially since T_{max} and P_{max} rarely coincide. Indeed, some zircon grains in high-grade metamorphic rocks may crystallise from partial melts generated at relatively low pressure during exhumation (e.g. Roberts and Finger 1997). A further constraint on the growth of zircon in metamorphic rocks is the availability of Zr. Fraser et al. (1997) suggest that the breakdown of Zr-bearing major minerals such as garnet, hornblende and biotite may yield significant quantities of Zr, although the transport of relatively insoluble Zr to a site of zircon growth remains problematical. In some cases a process of Ostwald ripening has been invoked (Vavra et al. 1999), or the zircon grows adjacent to the mineral which is breaking down (e.g. ilmenite, Bingen et al. 2001). One approach which can be used to relate zircon growth to P–T evolution paths is to study the trace-element composition of the zircon grains themselves, as well as other potentially key metamorphic minerals, for diagnostic signs of the involvement of specific metamorphic reactions. We present here ion-microprobe rare-earth element (REE), Y and Hf data which are closely integrated with detailed petrographic observations from zircon grains and garnets in garnet granulites from the Betic-Rif orogen of the western Mediterranean. These petrographic and geochemical data are used to argue that zircon growth was essentially synchronous with the latest growth phase in the garnet. This allows us to correlate the U–Pb age from the zircon grains to a specific, decompressional section of the P–T path recorded by this stage of garnet growth.

M.J. Whitehouse (✉)
Swedish Museum of Natural History,
Box 50007SE-104 05, Stockholm, Sweden
E-mail: martin.whitehouse@nrm.se
Tel.: +46-8-51954069
Fax: +46-8-51955169

J.P. Platt
Department of Geological Sciences,
University College London, Gower Street,
London, WC1E 6BT, UK

Editorial responsibility: I. Parsons

Geological setting

The high-grade metamorphic rocks surrounding the ultramafic massifs near Ronda in southern Spain and Beni Bousera in Morocco (Fig. 1) have long attracted attention and controversy. They were initially considered as relics of Variscan (Permo-Carboniferous) metamorphism (e.g. Kornprobst 1969), a view still held by some (e.g. Bouybaouène et al. 1998), but they were reinterpreted as forming the inner parts of zoned thermal metamorphic aureoles around solid-state ultramafic protrusions of Alpine (Miocene) age by Loomis (1972a, 1972b), primarily on the basis of K/Ar ages. Early Miocene Ar–Ar, Rb–Sr and fission-track cooling ages have since been reported by a number of workers (Zeck et al. 1992; Monie et al. 1994; Sosson et al. 1998). Structural and thermobarometric work has shown, however, that the interpretation of these zoned metamorphic complexes as thermal aureoles is untenable—changes in initial metamorphic pressure across them are at least as important as changes in temperature. They are now generally considered to be the result of drastic attenuation of an originally thick Alpine metamorphic sequence (Torres-Roldán 1981; Balanyá et al. 1993; Tubía et al. 1993; Vissers et al. 1995; Argles et al. 1999) associated with late orogenic extensional thinning of the internal Betic-Rif orogen (Platt and Vissers 1989). The timing of high-grade metamorphism, and the timing and rate of exhumation are, nevertheless, still subject to considerable discussion. Montel et al. (1995) have used the U–Pb age of monazite crystals included in garnet to argue for a Variscan age for initial granulite facies metamorphism, and Sánchez-Rodriguez (1998) makes a similar case based on a clustering of U–Pb ages from zircon cores. Sánchez-Rodriguez and Gebauer (2000), however, assume that 19.9 ± 1.7 Ma rims on zircons grains from associated, partially amphibolitised eclogites correspond to the time of maximum pressure during an Alpine subduction event which buried these rocks to depths of about 55 km. Based on Ar–Ar and fission-track ages in the range 19–20 Ma, they also suggest exhumation rates on the order of >31 km/10^6 years. Platt and Whitehouse (1999), on the other hand, found that large, unzoned, metamorphic zircon grains from the granulite-facies rocks around the Carratraca massif yield an age of 21.2 ± 0.7 Ma, proposing that these are essentially closure ages. They used thermal modelling to suggest that the rocks cooled below 800 °C at a depth of about 16 km, and calculated average exhumation rates of around 6 km/10^6 years.

The differences in opinion among these various workers arise largely from differences in the interpretation of the meaning of the zircon ages. Do the ages represent crystallization or cooling ages? At what time in the *P–T* evolution of the rocks did zircon grow, and when did Pb effectively cease to diffuse through the zircon structure? Resolution of these questions will fundamentally affect our understanding of the timing and significance of the high-grade metamorphism in the Betic-Rif orogen.

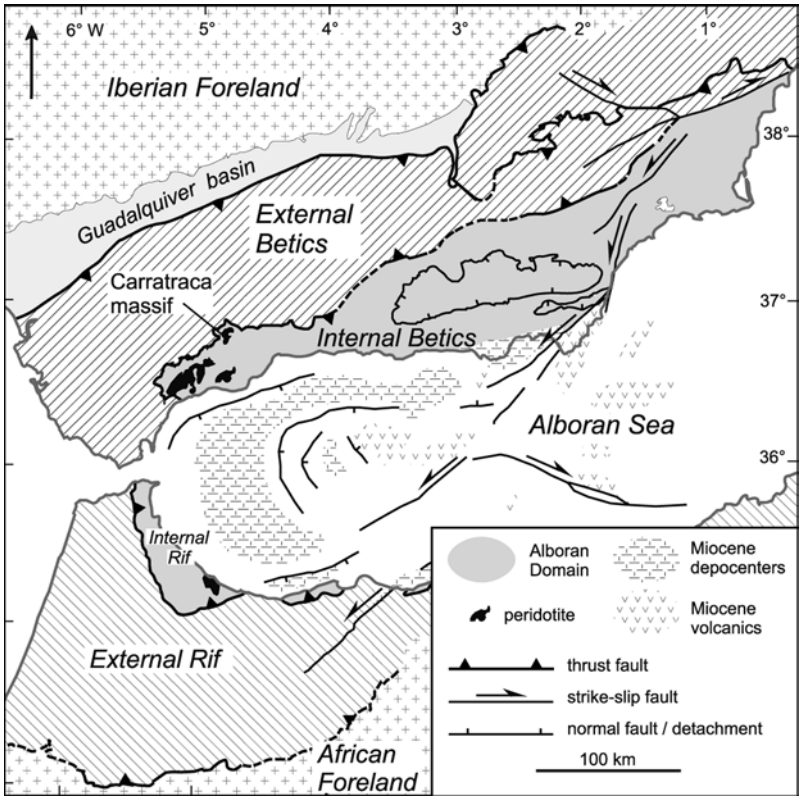

Fig. 1 Tectonic map of the Alboran Sea and the adjacent mountain belts, showing the location of the Carratraca peridotite massif and the sampled garnet gneiss. *External Betics* comprises thin-skinned Miocene thrust belts developed in Mesozoic–Tertiary platform and basin sequences on the southern rifted margin of Iberia. *External Rif* is the equivalent thrust belt on the northern rifted margin of Africa. The *Internal Betics* and *Internal Rif* zones, together with the crust beneath the Alboran Sea, constitute the Alboran Domain, a collisional terrain developed in Late Mesozoic–Palaeogene time from continental crustal fragments of uncertain provenance

The sample studied here (PB383) was taken from a layer of garnet gneiss up to 100 m thick lying on the north side of the Carratraca peridotite massif (Fig. 1; see also Platt and Whitehouse 1999 for further location details). The gneiss layer forms the highest-grade part of the zoned metamorphic complex lying structurally above this part of the Ronda peridotite sheet (Argles et al. 1999).

Petrography

Sample PB383 contains abundant (25% by volume) garnet porphyroblasts up to 4 cm in diameter, in a strongly foliated matrix of quartz–plagioclase–K-feldspar–garnet–sillimanite–biotite–ilmenite, including significant areas of leucosome development. Garnet cores are relatively clean, and contain a suite of coarse-grained, unoriented inclusions (kyanite–rutile–plagioclase–biotite), interpreted to represent an early high-pressure assemblage. Discontinuous outer zones, from zero to several millimetres in thickness, contain abundant inclusions of fibrous sillimanite (Fig. 2), and the garnets are mantled by sympletitic cordierite–anorthite–hercynite coronas (Platt et al., unpublished data) which are interpreted to have formed by garnet breakdown. Garnets have high-pyrope and low-grossular/-spessartine components. Fe/(Fe + Mg) profiles across the grains are remarkably flat, a feature observed by Argles et al. (1999) in similar Carratraca granulite samples which they attribute to high-temperature diffusional homogenisation. However, the rims rich in sillimanite inclusions commonly show grossular contents up to three times higher than the cores, which may reflect partial melting in the matrix during this stage of growth (Spear and Kohn 1996). The growth of sillimanite-bearing outer rims of the garnets is likely to be a result of fluid-absent breakdown of biotite (biotite + aluminosilicate + plagioclase + quartz = garnet + K-feldspar + liquid, Spear and Kohn 1996) during decompression or heating.

The sequence of assemblages in the garnet gneiss at this location was interpreted to represent a history of decompression from high-pressure granulite-facies conditions ($P = 12$–14 kbar, $T = 700$ °C) represented by the garnet cores, to $P = 4$ kbar, $T = 800$ °C represented by the cordierite–anorthite–hercynite reaction coronas (Argles et al. 1999). Thermobarometry is compromised, however, by diffusional homogenisation of garnet and disequilibrium reactions which occurred during decompression, and Platt et al. (unpublished data) have re-examined the P–T history based on assemblages in a boudin of mafic gneiss from the same outcrop as PB383, in which diffusional modification and decompressional modification was more restricted. They conclude that the rocks experienced a decompressional P–T path from around 11.7 ± 1.1 kbar, 730 ± 50 °C to 4.3 ± 1.5 kbar, 790 ± 60 °C. On this path the sillimanite-bearing garnet rims in PB383 must have grown at a pressure of less than 8.5 kbar, this being the pressure at which the path intersects the kyanite–sillimanite univariant curve. It is unlikely that garnet growth could have occurred at a pressure of < 4 kbar, as garnet of this composition would be unstable with respect to cordierite at this pressure, nor is it likely that it could grow under conditions of declining temperature (Spear and Kohn 1996). The rims therefore formed between 8.5 and 4 kbar under conditions of increasing T (Platt et al., unpublished data).

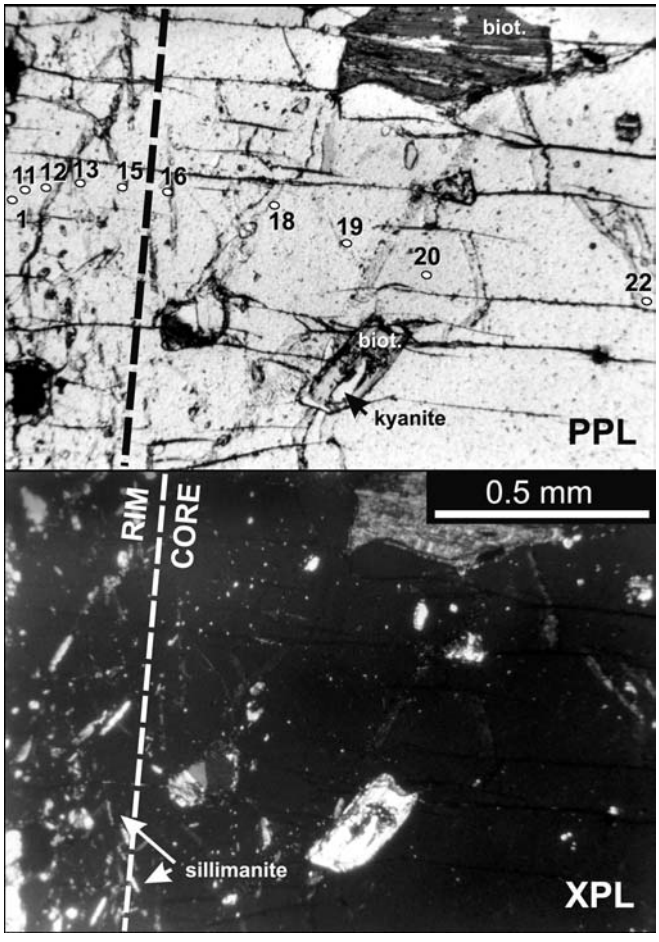

Fig. 2 Photomicrograph of a typical garnet from PB383, showing the development of sillimanite-bearing rims on kyanite-bearing cores (approximate boundary marked by *dashed line*). *Numbered spots* represent electron microprobe major-element and SIMS trace-element analytical locations on a detailed traverse of this grain

The zircon grains analysed from sample PB383 by Platt and Whitehouse (1999) were separated from crushed bulk rock and thus their precise petrographic environment is unknown, although the existence of both garnet- and matrix-hosted zircon was noted in thin section. In this study, in addition to analysing REEs, Y and Hf in a number of the zircon grains dated by Platt and Whitehouse (1999), we have taken two approaches to clarify their relation to the metamorphic petrography of sample PB383: (1) CL imaging of zircon grains in thin sections, and (2) SIMS U–Th–Pb and REE, Y and Hf analyses of zircons grains separated from a garnet

concentrate. In addition, complementary REE analyses of garnets have been performed in thin section. Detailed thin section analysis of PB383 (seven sections) was undertaken in order to better understand the petrographic setting of the zircon. Zircon grains were found in the matrix (dominant), cordierite–anorthite–hercynite reaction coronas after garnet, garnet rims and cores (rare).

Matrix-hosted zircon grains (Fig. 3, grains labelled "mtx") show identical characteristics to those previously studied by Platt and Whitehouse (1999), with a broadly homogeneous, structureless or patchily zoned, medium-grey cathodoluminescent growth phase forming rims, or sometimes the entire exposed section of the crystal. Cores (when present) display a range of structures from diffuse to sharp growth banding, suggestive of a primary igneous origin. Given the large amount of garnet in PB383, the dominance of matrix zircon in the thin sections suggests that most of the zircon grains analysed by Platt and Whitehouse (1999) may have been derived from the matrix. Platt and Whitehouse (1999) reported a Miocene age of 21.2 ± 0.7 Ma from nine analyses of the CL-homogeneous rim phase, with a range of $^{207}Pb/^{206}Pb$ ages from the cores of 480–950 Ma, consistent with their detrital origin from mixed source regions. Most of these core ages are discordant and therefore minimum ages.

CL images of zircon grains separated from the garnet concentrate are also shown in Fig. 3 (grains prefixed "G"). These show the same general features as the grains imaged in thin section and grains separated from the whole rock (see Platt and Whitehouse 1999; Fig. 4a), the latter possibly matrix-dominated, as argued above. Most of the zircon grains within the garnets which we examined in situ are small (< 100 μm), and largely confined to the sillimanite-bearing outer zones of the garnets and the cordierite–anorthite–hercynite coronas formed by garnet breakdown (Fig. 3, grains labelled "rim" and "rxn" respectively). These show distinct cores and narrow, homogeneous rims. The few zircon grains found in core regions of garnets appear to lack overgrowths (e.g. Fig. 3, grain 21).

On the basis of this CL imaging, we can confidently rule out the possibility that the homogeneous CL rims/grains formed entirely as the product of garnet breakdown. If this were the case, we would not expect to see similar features in both the garnet- and the matrix-hosted zircon, given their completely different petrographic/geochemical environment. In particular, the presence of CL-homogeneous rims on zircon grains

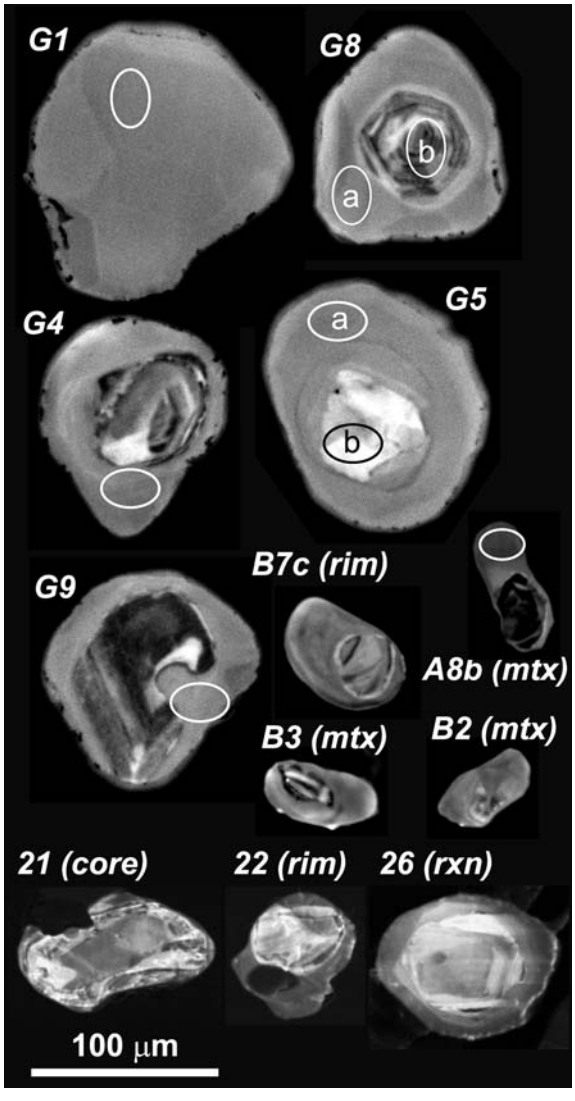

Fig. 3 Cathodoluminescence images of selected zircon grains from this study. Grains with the prefix *G* were separated from garnets; other grains were imaged directly in a polished thin section, with their petrographic locations indicated in *parentheses* (*mtx*. matrix, *rxn*. cordierite–anorthite–hercynite corona after garnet). Ion microprobe analytical sites (U–Pb and/or REEs) are indicated by *ellipses*

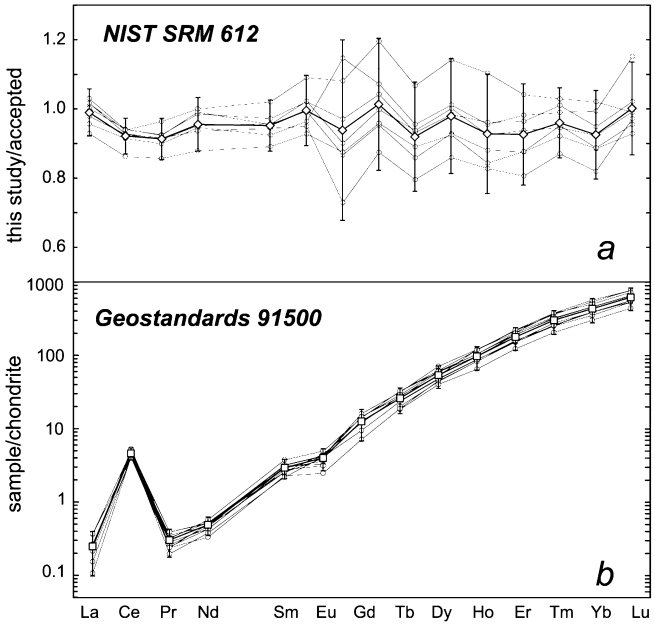

Fig. 4a, b REE analytical data for **a** NIST SRM 610, and **b** Geostandards zircon 91500, obtained using NIST 610 as a calibration standard. *Shaded lines* represent individual analyses; *squares* represent average with 2σ error bars indicated

both in garnet (rims), where they would have been armoured from metamorphic reactions, and in the matrix appears incompatible with their growth after garnet. Similarly, with specific reference to zircon hosted in the cordierite–anorthite–hercynite coronas, we consider it unlikely that these result from garnet breakdown because some process would then have to transport Zr to both matrix zircon as well as zircon armoured in unreacted garnet to generate identical features.

This textural analysis leaves the possibility that the zircon rims grew either before growth of the sillimanite-bearing garnet rims, in which case their Miocene age would provide a upper limit for the timing of high-*P* metamorphism, or synchronously with the growth of the sillimanite-bearing garnet rims.

Analytical methods

Determinations of all 14 REEs together with Y and Hf were made using a Cameca IMS1270 ion microprobe at the Swedish Museum of Natural History (Nordsim facility). Although this instrument is capable of a high mass resolution (MR, defined as M/ΔM at 10% peak height) at high transmission and is routinely used for U–Pb geochronology at MR of ca. 5,000, achieving the much higher resolution required to separate the heavy REEs from oxides of lighter REEs (MR ca. 10,000) results in substantial loss of transmission. In addition, there are only few, well-characterised zircon or garnet crystals available as calibration standards; for example, previous studies on the Geostandards zircon 91500 suggest some heterogeneity (Hoskin 1998). Analyses were therefore performed using low mass resolution and high-energy ions, following the method outlined by Hinton (1990) which discriminates against molecular species, in particular the interference of light REEs on heavy REEs. This method also minimises matrix effects, facilitating calibration of silicates against synthetic glass standards (Hinton and Upton 1991).

High-mass resolution (MR > 5,000) scans were performed using a ± 15 eV window across all peaks of interest in both the 91500 zircon and the NIST SRM 610 glass, at sample high voltage offsets of 0, −70, −100 and −120 V in order to assess the efficiency of energy filtering for removing interferences at each mass. A peak hopping routine was then established at a lower mass resolution (MR < 3,000), in which the light REEs (^{139}La, ^{140}Ce, ^{141}Pr, ^{144}Nd and ^{149}Sm) were analysed at −70 V, and the heavy REEs (^{159}Tb, ^{165}Ho, ^{166}Er, ^{169}Tm, ^{172}Yb and ^{175}Lu) at −100 V. An unidentified interference occurred on all abundant Gd isotopes in the NIST SRM 610 glass (but not zircon) at −100 V offset, requiring analysis of ^{160}Gd (+ ^{160}Dy) and ^{161}Dy at −120 V. In addition to the REE isotopes, the peak hopping routine included the following species (measured at −70 V offset unless otherwise stated): ^{30}Si as a matrix reference, ^{89}Y, mass ~88 to monitor for $^{176}Hf^{2+}$, ^{180}Hf (both −100 V offset), and $^{90}Zr^{28}Si^{16}O$ in order to correct ^{139}La, ^{140}Ce and ^{141}Pr for interferences from this abundant matrix species in zircon. Additional isobaric interference corrections were made for ^{144}Sm on ^{144}Nd, and ^{161}Dy on ^{160}Gd. Primary beam size, shape and ion current are the same as those used for U–Pb analysis of zircon (ca. 30 μm, slightly elliptical flat-bottomed crater, 4nA O_2^- current; Whitehouse et al. 1997).

Concentrations were calculated with reference to NIST SRM 610 glass (nominal 500 ppm), using the working values recommended by Pearce et al. (1996, their Table 8, "preferred average"). Analyses of NIST SRM 612 glass (nominal 50 ppm) calibrated against NIST SRM 610 show deviations up to ±20% in some of the middle REEs (Table 1, Fig. 4a). The average of seven analyses is generally in good agreement with the values recommended by Pearce et al. (1996, their Table 9). Large deviations in individual values about this average may reflect actual heterogeneities in NIST SRM 612 at the SIMS sampling scale.

Table 1 Ion-microprobe REE, Y and Hf analytical data for Geostandards zircon 91500 and NIST SRM 612 glass (concentrations in ppm)

Analysis ID	La	Ce	Pr	Nd	Sm	Eu	Gd	Tb	Dy	Ho	Er	Tm	Yb	Lu	Y	Hf
Geostandards zircon 91500 (development analyses)																
18	0.059	3.06	0.035	0.24	0.45	0.18	4.16	1.17	14.3	5.4	30	7.8	75	15.9	143	6,232
19	0.085	2.43	0.022	0.19	0.43	0.20	1.97	0.73	10.6	4.6	24	6.0	57	12.8	137	5,182
20	0.025	2.50	0.025	0.19	0.41	0.17	0.81	0.66	9.67	3.6	19	4.9	49	10.6	138	4,034
21	0.036	2.56	0.031	0.21	0.37	0.22	1.93	0.87	11.7	4.9	24	6.2	63	13.6	127	4,598
22	0.062	2.69	0.023	0.21	0.47	0.23	2.85	0.98	14.2	5.8	30	7.6	74	15.6	153	5,646
23	0.059	2.63	0.021	0.23	0.46	0.23	3.13	1.13	17.1	6.7	34	8.7	87	18.5	160	6,506
24	0.086	2.98	0.029	0.24	0.38	0.25	2.35	1.01	12.7	6.6	32	9.0	81	17.5	175	6,299
25	0.055	3.21	0.028	0.26	0.55	0.28	2.76	1.17	15.0	6.5	35	9.1	92	18.5	181	6,201
26	0.059	2.82	0.035	0.23	0.47	0.24	2.84	1.04	14.7	5.8	32	8.0		17.4	167	5,281
28	0.056	2.68	0.017	0.17	0.32	0.23	1.85	0.85	11.4	4.8	25	6.2	62	13.5	135	5,243
29	0.050	2.41	0.021	0.15	0.33	0.14	1.39	0.68	10.9	4.6	25	6.7	63	13.0	122	6,246
Geostandards zircon 91500 (this study)																
30	0.077	2.64	0.026	0.19	0.34	0.19	1.71	0.71	9.6	4.1	21.3	5.52	51	11.5	137	4,430
31	0.06	2.74	0.02	0.20	0.37	0.19	2.16	0.88	12.5	5.0	27	6.68	63.9	13.8	148	5,290
32	0.074	2.66	0.029	0.19	0.34	0.17	2.89	0.96	16.1	5.6	29.8	7.4	69.8	15.8	139	6,080
41	0.04	2.59	0.031	0.16	0.39	0.21	2.53	0.92	13	5.9	27.4	6.75	65.5	15.3	129	6,210
42	0.15	2.81	0.049	0.19	0.36	0.26	1.58	0.93	11.8	4.8	25.2	6.44	57.7	12.9	141	5,310
43	0.12	2.42	0.038	0.16	0.34	0.18	1.96	0.85	11	4.9	25.8	6.68	60.2	13.4	131	5,370
NIST SRM 612																
1	34.2	35.0	33.4	33.3	33.9	33.1	42.3	38.4	34.3	38.3	35.7	36.8	39.5	37.4	36.4	40.0
2	36.8	36.0	34.3	34.7	35.6	35.1	35.8	37.4	33.5	37.2	35.9	36.1	40.3	35.7	36.8	35.4
3	35.8	36.0	34.3	34.9	35.0	35.2	33.2	35.8	33.7	37.9	34.6	35.1	37.7	34.8	35.7	34.4
5	36.3	35.9	35.7	35.2	37.4	37.5	39.9	42.8	38.3	43.2	41.2	39.0	41.0	38.4	36.9	34.4
6	35.0	35.5	33.8	33.5	35.1	34.2	32.0	34.2	30.8	35.1	32.9	32.8	36.7	33.3	35.3	32.2
7	36.3	35.5	34.0	32.9	34.6	32.7	26.9	31.4	28.6	32.5	30.9	30.2	34.7	30.9	37.1	33.7
8	33.2	33.0	31.8	30.9	32.7	31.9	32.3	34.4	32.0	35.0	31.5	32.9	37.9	33.4	34.0	33.2

Eleven analyses of Geostandards 91500 zircon (Wiedenbeck et al. 1995) were performed during method development, (1) to monitor reproducibility between analytical sessions, and (2) for comparison with results from other SIMS and laser-ablation ICP-MS studies (Garbe Schönberg and Arpe 1997; Nesbitt et al. 1997; Hoskin 1998). The analyses from the 91500 zircon (Table 1, Fig. 4b) show an expected, smooth increase in chondrite-normalised values of trivalent REEs as ionic radius decreases from La to Lu, together with large positive Ce anomaly and small negative Eu anomaly. Good agreement is obtained between the SIMS measurements for zircon 91500 presented here and both the SIMS and LA-ICP-MS analyses of Hoskin (1998) and the LA-ICP-MS analyses of Nesbitt et al. (1997; excepting the very low La in the latter study). A further six measurements of zircon 91500 were made during this study and are indistinguishable from earlier analyses (Table 1).

Analytical errors on individual REE determinations depend upon element concentration, abundance of the isotope chosen for measurement, and instrument sensitivity in a given analytical session. For zircon cores with chondrite-normalised REE profiles similar to those of the Geostandards zircon 91500, the average analytical error ranges from ca. ±10% (1σ) for the light REEs (except Ce in zircon which is typically ca. ±3%) to ca. ±5% for most of the other REEs. Heavy REEs from zircon rims and garnets with relatively flat Gd–Lu profiles have errors of ca. ±10–15%. Errors on Y and Hf are typically ca. ±2 and ±4% (1σ) respectively at the abundance levels encountered.

SIMS U–Th–Pb analyses presented here were performed using the same analytical procedures as those reported by Whitehouse et al. (1997, 1999) and Platt and Whitehouse (1999). Analytical errors on $^{206}Pb/^{238}U$ ratios include a component propagated from repeated measurements on the ca. 1,065 Ma Geostandards zircon 91500, and $^{207}Pb/^{206}Pb$ errors are the largest of the Poisson counting errors or the observed analytical error. Common Pb is assumed to have the composition of modern terrestrial Pb (Stacey and Kramers 1975) following the rationale of Zeck and Whitehouse (1999). Age calculations assume the decay constants of Steiger and Jäger (1977).

Electron microprobe analyses of garnets were performed using a Jeol 733 Superprobe, with an Oxford Instruments ISIS energy dispersive system. Data were collected at 15 kV for 100 s count time with a 2 μm spot. The derived grossular content and Fe/(Fe + Mg) are given in Table 2.

Refined U–Pb geochronology of PB383

An additional nine U–Th–Pb analyses were made on the CL-homogeneous rims/grains separated from the garnet concentrate. These are presented in Table 3 and Fig. 5 along with data previously presented by Platt and Whitehouse (1999); analysis locations are shown in Fig. 3. Seven of these grains yield Miocene ages. Of the two older ages, G4 (ca. 63 Ma) may include a component of the core whereas G2 (concordant at ca. 1,790 Ma) probably represents an older detrital grain which coincidentally shares the morphology of the Miocene grains. It is clear from Fig. 5 that, within the limits

Table 2 Ion-microprobe REE, Y and Hf analytical data forPB383 zircons and garnets (concentrations in ppm)

Grain no.	Structural class[a]	La	Ce	Pr	Nd	Sm	Eu	Gd	Tb	Dy	Ho	Er	Tm	Yb	Lu	Y	Hf
Zircons from bulk rock																	
3	Rim/no struct	0.116	7.54	0.295	4.65	6.36	0.642	13.7	1.74	7.85	1.05	2.2	0.324	3.33	0.466	24.4	12,900
4	Rim/no struct	0.111	8.76	0.335	5.42	7.96	0.997	22	2.9	15.1	1.98	4.34	0.512	6.48	0.81	43.8	12,200
8a	Rim/no struct	0.13	1.32	0.094	1.05	2.81	0.181	19.8	4.44	27.8	3.95	9.06	1.04	10.6	2.07	102	12,600
8c	Core	0.232	48.5	0.236	2.3	3.92	0.867	31.3	8.84	123	36.3	168	35.5	306	67.6	912	11,000
7a	Rim/no struct	0.131	0.738	0.06	0.634	2.64	0.17	9.19	2.38	10.7	1.77	3.12	0.572	4	0.801	72.5	7,210
7b	Core	1.27	40.5	1.28	5.03	7.58	2.58	26.8	9.82	101	38.6	170	35.5	300	65	1,380	7,960
Zircons from garnet concentrate																	
G1	Rim	0.162	8.14	0.212	2.73	3.69	0.438	6.85	1.05	4.38	0.607	1.42	0.177	1.87	0.42	14.4	11,700
G8a	Rim	0.197	8.89	0.409	6.52	8.37	0.897	15.3	2.18	10.9	1.7	4.29	0.514	5.77	0.933	38.5	11,400
G8b	Core	0.165	38	0.126	1.06	1.87	0.753	13.2	4.4	55.6	20	95.4	23.1	214	57.4	500	12,500
G5a	Rim	0.17	3.45	0.155	2.33	4.57	0.324	14.1	2.12	10.8	1.49	3.6	0.444	5.52	0.855	36.4	12,400
G5b	Core	0.159	25.9	0.159	1.51	2.65	0.557	15.6	5.09	52.8	20.7	86.9	18.2	174	43.4	505	11,000
Zircon analysed in thin section																	
TSB-8b	Rim (matrix)	0.047	1.24	0.041	1.2	3.47	0.272	12.6	3.5	22.6	3.18	7.87	1.01	6.12	2.32	116	10,200
Garnet analysed in thin section																	
gt-B1	Intermediate	0.001	0.061	0.134	5.2	4.82	0.811	12.8	4.74	44.8	12.7	41.1	5.31	41.3	7.5	382	9.78
gt-B-c	Centre	0.013	0.084	0.109	5.42	8.79	1.05	23.9	10.2	99	24.4	68.7	11.4	91.3	14.9	542	17.4
gt-B-r	Rim	0.007	0.238	0.247	7.99	17.9	1.79	42.9	8.3	52.4	4.16	8.83	0.72	10.3	2.12	85.4	6.62
garbig1	Trav.(0, 0.69, 0.28)					11.5	0.799	27.1	3.49	16	2.29	4.17	0.677	8.01	1.12		
garbig1b2	Trav.(0)					9.52	0.654	20.9		13.7		3.54	0.514		1.11		
garbig1b3	Trav.(0)					19.7	2.14	22.9		11.8		3.32	0.4		0.76		
garbig1b4	Trav.(0)					7.97	0.491	17.7		12.1		3.08	0.441		0.742		
garbig11	Trav.(34, 0.69, 0.31)					13.7	1.03	21.6		12.9		4.7	0.731		1.19		
garbig12	Trav.(88, 0.68, 0.33)					13.8	1.11	19.4	2.94	15.6	2.31	5.37	0.804	7.27	1.22		
garbig13	Trav.(173, 0.67, 0.33)					13.5	1.48	16.4	3.64	19.7	3.34	6.69	0.933	7.94	1.32		
garbig15	Trav.(276, 0.67, 0.28)					10.8	1.27	13.3	4.15	24.2	4.63	9.76	1.24	9.76	1.69		
garbig16	Trav.(389, 0.67, 0.18)					5.77	0.982	9.82	3.18	26.9	4.35	13	2.08	12.9	2.64		
garbig18	Trav.(654, 0.68, 0.22)					6.12	0.939	13.1	4.55	38.5	7.27	22.7	3	20.2	3.84		
garbig19	Trav.(842, 0.68, 0.16)					3.7	0.79	11.8	6.05	58.4	16.8	53	8.42	56.8	9.22		
garbig20	Trav.(1,046, 0.68, 0.16)					3.61	0.654	12.1	6.71	74	24	83.7	14.5	98.6	16.2		
garbig22	Trav.(1,600, 0.68, 0.12)					1.81	0.483	17.6	12.6	140	50.7	153	26.2	204	27.2		

[a]For traverse analyses, numbers in parentheses indicate distance (μm) from the edge of the garnet, Fe/(Fe + Mg) and grossular content (formula units) respectively (complete garnet major-element analyses available on request)

Table 3 Ion-microprobe U–Th–Pb data forsample PB383 (data are sorted according to $^{206}Pb/^{238}U_{corr}$ age[f]; errors are 1σ)

Analysis[a]	Character[b]	U (ppm)	Pb (ppm)	Th/U[c]	$^{206}Pb/^{204}Pb$	f_{206}[d] (%)	$^{207}Pb/^{206}Pb$	$^{206}Pb/^{238}U$	Disc[e] (%)	$^{207}Pb/^{206}$ Pb age (Ma)	$^{206}Pb/^{238}U$ age (Ma)	$^{206}Pb/^{238}U_{corr}$ age[f] (Ma)
13	*eu-r-s-uz*	*419*	*1.5*	*0.30*	*629*	*0.00*	*0.0632 ± 0.0038*	*0.00308 ± 0.00010*			*19.9 ± 0.7*	*19.4 ± 0.7*
G5	sub-r-o-uz	134	0.5	0.29	1,930	0.09	0.0585 ± 0.0035	0.00312 ± 0.00008			20.1 ± 0.5	19.8 ± 0.5
10	*sub-r-s-uz*	*347*	*1.2*	*0.24*	*> 1e6*	*0.30*	*0.0459 ± 0.0026*	*0.00315 ± 0.00009*			*20.2 ± 0.6*	*20.3 ± 0.6*
16	*sub-r-s-uz*	*334*	*1.2*	*0.21*	*1,390*	*0.00*	*0.047 ± 0.0028*	*0.00320 ± 0.00009*			*20.6 ± 0.6*	*20.6 ± 0.6*
4	*an-r-s-uz*	*401*	*1.4*	*0.26*	*4,110*	*0.10*	*0.0457 ± 0.0024*	*0.00321 ± 0.00009*			*20.7 ± 0.6*	*20.7 ± 0.6*
15	*an-r-s-uz*	*804*	*2.8*	*0.08*	*1,190*	*10.3*	*0.0518 ± 0.0017*	*0.00327 ± 0.00009*			*21.0 ± 0.6*	*20.9 ± 0.6*
G3	sub-r-o-uz	387	1.4	0.19	3,910	3.38	0.0483 ± 0.0020	0.00328 ± 0.00007			21.1 ± 0.4	21.1 ± 0.4
G1	an-r-s-uz	301	1.2	0.40	8,950	0.84	0.0484 ± 0.0019	0.00328 ± 0.00007			21.1 ± 0.5	21.1 ± 0.5
G6	an-r-s-uz	367	1.4	0.21	1,090	1.13	0.0473 ± 0.0018	0.00330 ± 0.00007			21.2 ± 0.5	21.2 ± 0.5
G8a	sub-r-o-uz	282	1.1	0.33	558	2.35	0.0473 ± 0.0020	0.00330 ± 0.00007			21.3 ± 0.5	21.2 ± 0.5
2	*sub-r-s-uz*	*405*	*1.5*	*0.31*	*4,010*	*2.93*	*0.0463 ± 0.0025*	*0.00331 ± 0.00009*			*21.3 ± 0.6*	*21.3 ± 0.6*
3	*sub-r-s-uz*	*354*	*1.4*	*0.23*	*2,060*	*0.52*	*0.0496 ± 0.0026*	*0.00336 ± 0.00009*			*21.7 ± 0.6*	*21.6 ± 0.6*
9	*sub-r-s-uz*	*333*	*1.3*	*0.39*	*6,010*	*1.06*	*0.0443 ± 0.0022*	*0.00336 ± 0.00009*			*21.7 ± 0.6*	*21.7 ± 0.6*
14	*an-r-s-uz*	*324*	*1.4*	*0.61*	*1,620*	*0.56*	*0.0485 ± 0.0029*	*0.00340 ± 0.00009*			*21.9 ± 0.6*	*21.8 ± 0.6*
6	*sub-r-s-uz*	*453*	*1.8*	*0.29*	*1,400*	*1.87*	*0.0514 ± 0.0019*	*0.00340 ± 0.00010*			*21.9 ± 0.6*	*21.7 ± 0.6*
G7	an-r-s-uz	450	1.7	0.12	2,810	0.50	0.0461 ± 0.0015	0.00343 ± 0.00007			22.1 ± 0.5	22.1 ± 0.5
G9a	an-r-o/mix-uz	302	2.2	0.10	18	2.45	0.0589 ± 0.0019	0.00657 ± 0.00013			42.2 ± 0.8	41.5 ± 0.8
1a	*sub-r-o-uz*	*171*	*1.3*	*0.11*	*3,900*	*1.73*	*0.0477 ± 0.0023*	*0.00717 ± 0.00011*			*46.1 ± 0.7*	*46 ± 0.7*
G4a	sub-r-o-uz	302	3.2	0.07	5,950	2.53	0.0521 ± 0.0016	0.00991 ± 0.00023			63.6 ± 1.5	63.2 ± 1.5
8a	*sub-r-o-uz*	*236*	*3.2*	*0.09*	*3,280*	*0.73*	*0.0537 ± 0.0017*	*0.0124 ± 0.0003*			*79.4 ± 2.1*	*78.8 ± 2.1*
7a	*eu-r-o-uz*	*221*	*7.9*	*0.07*	*2,010*	*4.13*	*0.052 ± 0.0011*	*0.0332 ± 0.0009*		*285 ± 48*	*210 ± 6*	*210 ± 6*
17	*sub-r-s-uz*	*268*	*11.8*	*0.06*	*4,790*	*0.27*	*0.0512 ± 0.0009*	*0.0410 ± 0.0011*		*252 ± 40*	*259 ± 7*	*259 ± 7*
8c	*c-z*	*304*	*23.8*	*1.68*	*7,520*	*0.44*	*0.0597 ± 0.0015*	*0.0507 ± 0.0015*		*593 ± 54*	*319 ± 9*	*316 ± 9*
12	*an-r-c-z*	*106*	*6.9*	*0.58*	*4,420*	*1.44*	*0.0656 ± 0.0016*	*0.0541 ± 0.0015*		*795 ± 52*	*339 ± 9*	*334 ± 9*
1b	*c-z*	*1,064*	*77.6*	*0.59*	*7,360*	*0.00*	*0.0592 ± 0.0011*	*0.0600 ± 0.0016*		*574 ± 41*	*375 ± 10*	*373 ± 10*
5	*an-r-c-z*	*136*	*9.7*	*0.43*	*2,360*	*1.86*	*0.0566 ± 0.0009*	*0.0601 ± 0.0016*		*475 ± 33*	*376 ± 10*	*375 ± 10*
11	*c-z*	*190*	*19.5*	*0.59*	*6,580*	*0.86*	*0.06918 ± 0.00064*	*0.0831 ± 0.0023*	*−37*	*904 ± 19*	*514 ± 14*	*507 ± 14*
7b	*c-z*	*812*	*117.0*	*0.86*	*5,240*	*3.32*	*0.07053 ± 0.00028*	*0.102 ± 0.003*	*−31*	*944 ± 8*	*627 ± 16*	*620 ± 17*
G2	an-r-s-uz	30	16.9	2.07	> 1e6	4.48	0.109 ± 0.002	0.318 ± 0.006		1,789 ± 28	1,780 ± 30	1,780 ± 30

[a]Italicised data have been presented previously (Plattand Whitehouse 1999) but have been recalculated using new error propagation routines applicable to the other data presented in this study. Prefix "G" indicates that the zircon grain was separated from a garnet concentrate

[b]Characteristics of analysed grain based upon CL and optical investigation. Abbreviations: external grain morphology: eu, euhedral;sub, subhedral; an, anhedral; p, prismatic/elongate; r, rounded/irregular; zonation: c, core; o, outer; s, single phase; z, oscillatory and/or sector zoned; uz, unzoned

[c]Calculated from measured ThO intensity

[d]Percentage of common Pb detected, calculated from measured ^{204}Pb and assuming 0 Ma, Stacey and Kramers (1975) average terrestrial Pb. No common Pb corrections have been applied to ratios reported in this table

[e]Degree of discordance (%); not reported for analyseswhich are concordant within 2σ error limits

[f]Concordia age calculated from uncorrected ratios assuming 0 Ma, Stacey and Kramers (1975) average terrestrial Pb ("^{207}Pb-corrected" age)

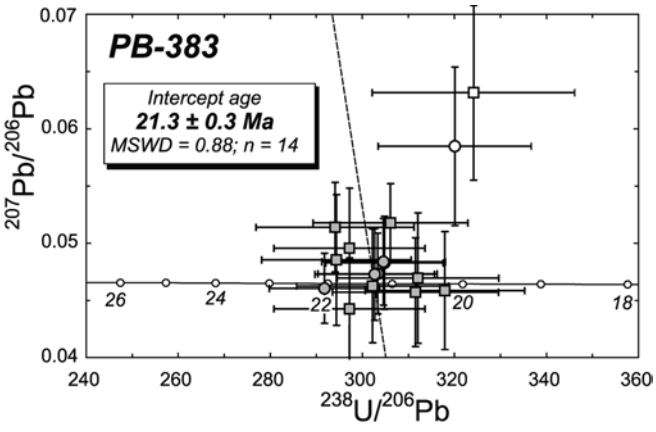

Fig. 5 Inverse concordia (Tera-Wasserburg) diagram showing U–Pb zircon data from sample PB383; *squares* are data from Platt and Whitehouse (1999); *circles* are new analyses on garnet-hosted zircon grains. Error bars are 2σ. The age of 21.3 ± 0.3 Ma (2σ) has been calculated by regressing the data together with a common Pb composition assumed to be equivalent to modern terrestrial Pb (Stacey and Kramers 1975), with an arbitrarily assigned error ($^{207}Pb/^{206}Pb = 0.83 \pm 0.1$). Two analyses which plot above concordia (*unshaded symbols*) are omitted from this calculation

of analytical uncertainty, there is no discernable age difference between the garnet-hosted zircon grains and those analysed from the whole rock. The latter, as argued above, is presumed to be dominated by matrix-hosted grains. Combining these two sets of U–Pb data, we calculate a concordia intercept age for the zircon rims in PB383 of 21.3 ± 0.3 Ma (95% confidence; $n = 14$, 2 rejections; MSWD = 0.89). This age is essentially identical to, but more precise than the 21.2 ± 0.7 Ma reported by Platt and Whitehouse (1999).

Geochemistry

Zircon REE, Y and Hf geochemistry

Chondrite-normalised REEs (Fig. 6a) from PB383 zircon grains reveal a striking difference between cores and rims. Cores exhibit profiles with strongly depleted light relative to heavy REEs, together with pronounced positive Ce and minor negative Eu anomalies. Such patterns are generally encountered in zircon of igneous origin (Hinton and Upton 1991; Barbey et al. 1995) and, with the exception of Ce and Eu, reflect the increasing ability of the zircon lattice to accommodate trivalent REEs as ionic radius decreases (from La to Lu). The positive Ce anomaly in igneous zircon probably results from favourable incorporation of small quantities of Ce^{4+} which may be present in the melt (Schreiber et al. 1980), whereas the negative Eu anomaly may reflect a Eu-depleted melt due to plagioclase fractionation. Relative to the cores, the rims show similar patterns of increasing enrichment from La to Gd, but the heavy REEs (Gd–Lu) are strongly depleted, with the most extreme depletion at Tm. These data indicate that the environment in which the zircon rims crystallised was depleted in HREEs relative to LREEs, requiring a mineral phase with complementary HREE enrichment which crystal-

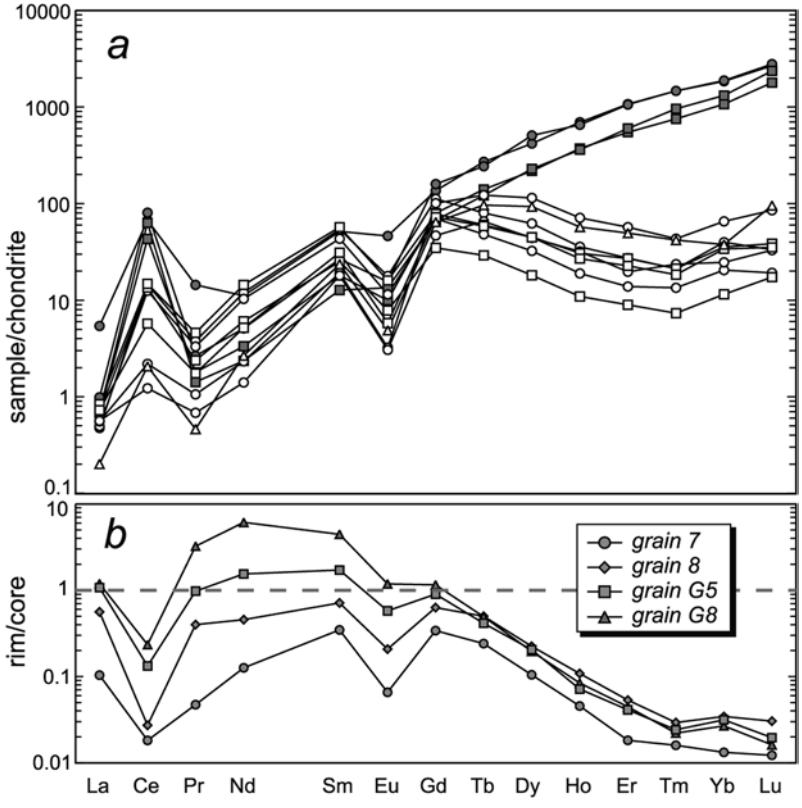

Fig. 6a, b Plots of REE data for zircon grains from PB383. **a** Chondrite-normalised (using the chondrite values of Anders and Grevesse 1989); *open symbols* represent rims analyses, *closed symbols* are from cores. **b** Rim normalised to core for zircon grains for which both core and rim analyses have been made

lised either in equilibrium with the zircon rims or prior to their development, strongly depleting the remaining rock in HREEs. The most abundant HREE-enriched phase in PB383 is garnet which, as we have argued above, is unlikely to have crystallised before the zircon. If garnet is responsible for the heavy-REE depletion, then the presence of strongly HREE-depleted zircon rims further suggests that the garnet growth is unlikely to postdate the zircon rim growth. A similar role for garnet controlling HREE distribution in metamorphic zircon has also been proposed by Bea et al. (1997) from Ivrea-Verbano, and Schaltegger et al. (1999) from the Vosges mountains. Recently, Rubatto (2002) has estimated trace-element (including REE) distribution coefficients between zircon and garnet and has used these to determine the timing of metamorphic zircon growth relative to zoned garnet in the Sesia-Lanzo zone.

Growth of zircon in a metamorphic rock requires a supply of Zr, either from unstable Zr-bearing phases which are reacting out (e.g. biotite, hornblende), from dissolution and re-precipitation of the zircon in situ (Fraser et al. 1997), or via a process of Ostwald ripening (Vavra et al. 1999). The REEs may also be provided to newly formed zircon either from reactions elsewhere in the rock, with transport to the site of crystallisation, or from in-situ, dissolved and re-precipitated zircon. In Fig. 6b we show the REE profiles for four zircon rims from PB383 normalised to their respective core analyses. Two of the rim analyses show an overall depletion of all REEs relative to their cores; the other two analyses also show depletions for most of the REEs but exhibit significant enrichments in Nd, Sm and, in one case, Pr. Smaller enrichments may also be observed in La and Gd. One possible explanation of these data is that in-situ dissolution and later re-precipitation has occurred with the dissolved zircon representing a pre-existing, more REE-enriched phase developed on the core during a pre-Miocene metamorphic and/or anatectic event in the zircon source rock. Subsequent re-precipitation in equilibrium with garnet would yield the overall HREE depletion observed in all rims but preserve (to a large extent) former higher levels of light–middle REEs. However, since none of the zircon cores show evidence in CL imaging for polyphase zircon growth, we prefer to attribute the enrichment of some of the REEs in the rims to local influx from elsewhere in the rock, requiring a fluid transport mechanism.

Bau (1996) has proposed that ratios of pairs of elements with similar charge and ionic radius may be used to distinguish minerals which have grown from or been modified by pure silicate melts and possess chondritic ratios, from those grown from or modified by aqueous fluids, the latter showing anomalous behaviour as a result of complexing effects (Bau calls this *Char*ge *Ra*tio *C*ontrol or ChaRaC). Two such ChaRaC ratios are Y/Ho (trivalent, ionic radii in 6-fold coordination ca. 104 pm) and Zr/Hf (quadrivalent, ionic radii in 8-fold coordination ca. 98 pm), which are plotted against each other in Fig. 7, with the ChaRaC field (i.e. chondritic ratios) defined by Bau (1996) shown for reference. All but one of the analysed Miocene rims fall within the ChaRaC field. In the ChaRaC model, this would be consistent with crystallisation from a silicate melt, with no indication of a significant role for aqueous fluids in the development of this zircon phase. Given our petrographic and geochemical observations which are interpreted to record the onset of decompression partial melting, the possibility of crystallisation from a silicate melt seems quite likely, although we stress that the ChaRaC model has not been tested for its applicability to a metamorphic environment, and such inferences must be treated with caution. Regardless of the significance of the ChaRaC model to this particular case, one of the analysed zircon grains (grain 7 from the whole-rock separate) behaves quite differently. For this grain, the Y/Ho and Zr/Hf ratios for both the older core and the Miocene rim plot close together but well outside the ChaRaC field (Fig. 7). A possible explanation for both these observations is that long-distance element transport suggested by MREE enrichment (via a silicate melt phase?), and local element derivation suggested by non-ChaRaC behaviour of grain 7 (e.g. from dissolution followed by re-precipitation) may be operating simultaneously, with local variations in the dominance of a particular mechanism, depending on petrographic environment.

Garnet REE geochemistry

To investigate further the role of garnet in the REE geochemistry of PB383 zircon grains, we have performed in-situ ion-microprobe REE analyses of garnet grains in polished thin sections (Table 2). We have analysed complete REEs + Y in a central part, a rim and a more intermediate position in one large grain (ca. 4 mm; garnet "B", Fig. 8a). Analyses from all parts of garnet

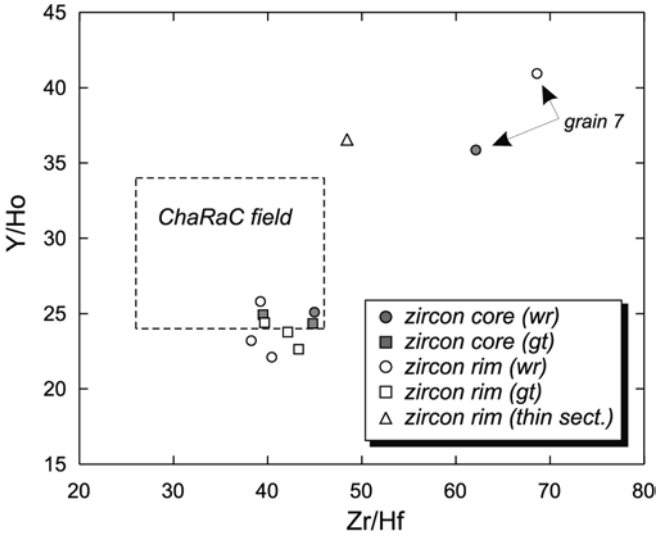

Fig. 7 Plot of Y/Ho ratio against Zr/Hf ratio for PB383 zircon grains. *Dashed line* represents the Charge-Radius-Controlled (*ChaRaC*) field defined by Bau (1996)

"B" are characterised by sub-parallel, steeply positive LREE profiles from ca. 0.01–0.1 times chondritic La to ca. 10–100 times chondritic Sm, with slightly higher abundances in the rims, as well as moderate negative Eu anomalies. In marked contrast to the similarity of the LREE profiles from different parts of the garnet, the MREEs–HREEs show a transition from relatively flat, ca. 100 times chondritic Sm–Lu profiles in the central analysis, to lower-abundance, negatively sloping Gd–Lu in the rim profile (Fig. 8a).

MREEs–HREEs (Sm to Lu) have been analysed from another large grain along a spot traverse line from the garnet core to rim (garnet "GARBIG"; Fig. 8b; analytical locations in Fig. 2). Determinations of LREEs were omitted from these analyses on the basis of the experience with garnet "B" which shows that they are relatively undiagnostic. Figure 9c shows analyses from "GARBIG" normalised to the garnet core analysis. MREE–HREE analyses from the GARBIG traverse (Figs. 8b, 9c) record in greater detail the transition which occurs across the garnet from core to rim. HREEs from Dy to Lu show a progressive decrease in abundance as the garnet margin is approached, with the greatest degree of depletion of rim relative to core occurring in the heaviest REEs (ca. 0.02 times for Tm–Lu, compared with ca. 0.1 times for Dy). Tb and Gd show slight decreases in abundance relative to the core (ca. 0.25 and 0.5 times respectively) until the nominal core–rim boundary is reached (Fig. 2), after which the abundance of Tb remains relatively constant whereas that of Gd increases progressively towards the margin. This behaviour results in sharp increases in ratios of Gd to the HREEs across the garnet rim (e.g. Gd/Dy). Sm and Eu record a progressive increase in abundance across the entire traverse, interestingly mirroring precisely the behaviour of Ca (shown by grossular content in Fig. 9a), even to the small fluctuation in the otherwise smooth patterns which is observed at ca. 700 μm from the rim.

In detail, these patterns are very similar to those described by Bea et al. (1997) for granulite-facies metapelites in a prograde sequence from Ivrea-Verbano, Italy. The marked decrease of HREEs and Y seen in the Ivrea-Verbano metapelites is attributed by Bea et al. (1997) to the increasing modal proportion of garnet acting as a HREE + Y repository as metamorphism progresses, including those elements released by the breakdown of xenotime (Bea and Montero 1999). The similar marked decrease in the garnet rim analyses of our sample PB383 may also be explained by early garnet growth reducing the amount of HREE + Y available for later growth. Furthermore, the progressive nature of the depletion appears compatible with continuous growth and/or reaction processes. We suggest here that garnet plays a similar role in controlling the availability of HREEs for zircon in PB383, with their strong depletion (Fig. 6) implying crystallisation in a HREE-poor environment, either synchronously with, or after growth of the garnet rims. Taken together with the arguments made above, on the basis of CL imaging and petrographic environ-

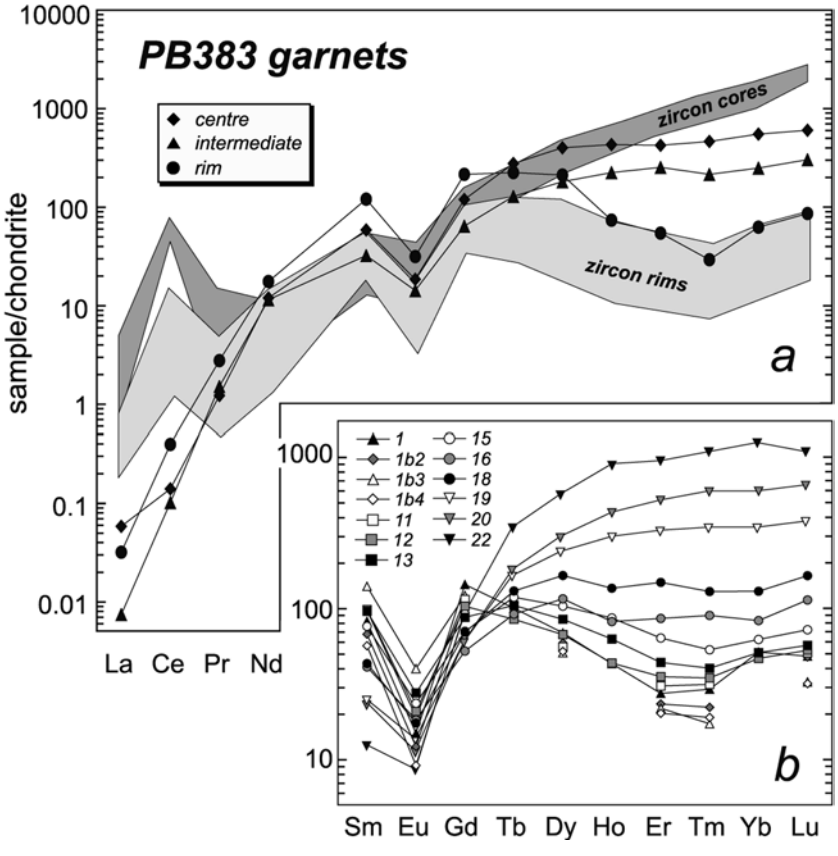

Fig. 8a, b Chondrite-normalised REE data from PB383 garnets. **a** Complete REE profiles from central, intermediate and rim locations of garnet "B". *Shaded fields* show ranges of zircon core and rim analyses from Fig. 5 for comparison. **b** Profiles for middle–heavy REEs (Sm–Lu) obtained on a traverse across garnet "GARBIG" (see Fig. 2). Note that analyses *1b2*, *1b3* and *1b4* were made at the extreme edge of the garnet and are further from the core than analysis *1*, the latter representing the closest analysis to the garnet edge for which major-element data have been obtained

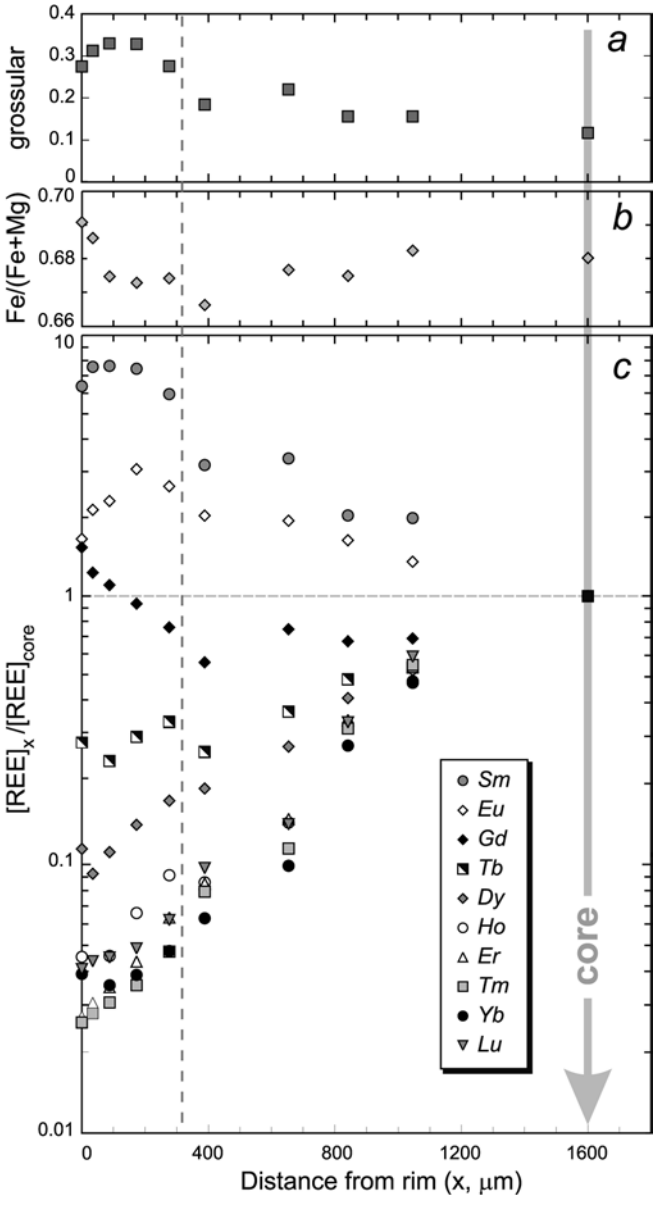

Fig. 9a–c Plot of selected elemental data from garnet "GARBIG" traverse. **a** Grossular content in formula units. **b** Fe/(Fe+Mg) ratio. **c** REE data normalised to the concentration for each element at the starting point of the traverse (point 22 in Fig. 2). Vertical *dashed line* represents the approximate position of the boundary between the garnet core and rim

ment, that zircon is unlikely to have crystallised after garnet, we suggest that the zircon rims grew contemporaneously and in near-equilibrium with the HREE-depleted garnet rims. The U–Pb age of 21.3 ± 0.3 Ma therefore represents a reliable proxy for growth of the garnet rims.

Implications of MREE enrichment in garnets

The relative enrichment of the MREEs in the rims of garnets from PB383, as well as the sharp increase in Gd/Dy ratios are similar to progressive changes observed with increasing pressure by Bea et al. (1997) in Ivrea-Verbano metapelites. In the latter case, Bea et al. (1997) attribute these changes to a $3^{x}M^{2+} \Leftrightarrow 2^{x}REE^{3+} + {}^{x}$ vacancy substitution which decreases the garnet unit cell dimension with increasing pressure, paradoxically favouring the incorporation of *larger* REE ions. These authors further suggest that Gd/Dy ratios in garnet may be used as a reliable indicator of pressure in metapelitic rocks, provided that the garnets meet the following criteria: (1) coexistence with modal monazite, (2) equilibration in a pressure range of 4–9 kbar, and (3) unit cell < 11.46 Å. Although we have observed modal monazite and suspect crystallisation in the appropriate pressure range for this barometer, the unit cell dimensions for garnets from PB383 exceed the proposed criteria (unit cells for all analysed PB383 garnets range from 11.48 to 11.54 Å, using the formula and coefficients provided by Bea et al. 1997), primarily because of the much higher grossular component in PB383. Thus, although Gd/Dy increases dramatically across the garnet rim, calculation of pressure using the Bea et al. (1997) model is, in this particular case, inappropriate. In addition, aforementioned textural evidence points to formation of the garnet rims during decompression, which is the opposite of that implied by increasing Gd/Dy ratios under the Bea et al. (1997) model. We therefore propose an alternative mechanism for MREE enrichment, in which a larger unit cell is thermodynamically favoured by decompression and higher Ca content, thus permitting incorporation of larger MREEs via the vacancy substitution.

Applicability of zircon/garnet partition coefficients

In a recent study Rubatto (2002) used the trace-element geochemistry of zircons growing in equilibrium with unzoned garnet to estimate partition coefficients between these two minerals ($^{REE}D_{zir/gt}$). These partition coefficients were then used to determine the timing of metamorphic zircon growth relative to a specific part of the zoned garnet in an eclogitic sample from the Sesia-Lanzo Zone of the Alps. In our study, detailed petrography together with geochemistry shows that the strongly HREE-depleted metamorphic zircon rims of sample PB383 grew at the same time as the garnet rims. Given the difference in major-element composition of the garnets in our study (Ca-enriched rims relative to cores, CaO∼4 wt%; Mg#∼0.3) and those of Rubatto (2002; Ca-depleted rims relative to cores, CaO∼4 wt%; Mg#∼0.1), it is instructive to use the data from our study to investigate the general applicability of the estimated $^{REE}D_{zir/gt}$ values. Figure 10 shows the REE partition coefficient calculated from the average REE composition of the PB383 metamorphic zircon rims and each point on the traverse of garnet "GARBIG". This diagram shows that the closest approximation to the equilibrium $^{REE}D_{zir/gt}$

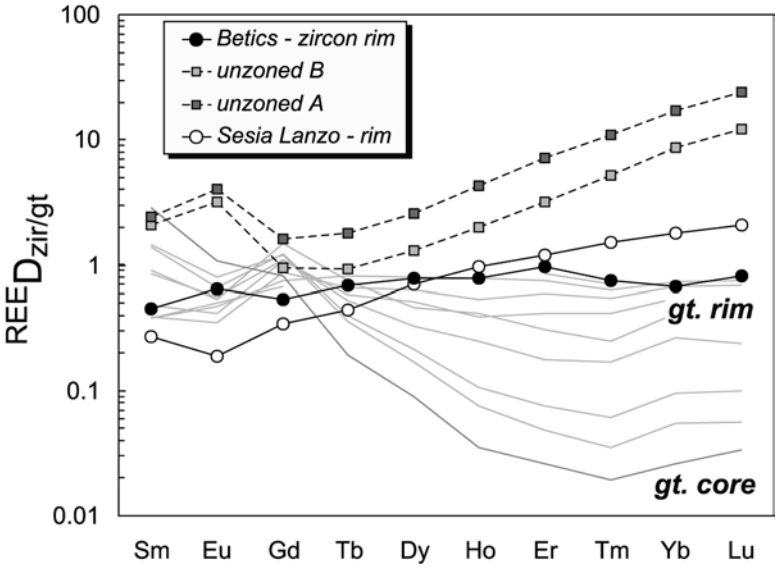

Fig. 10 Estimated zircon/garnet distribution coefficient ($^{REE}D_{zir/gt}$) for the MREEs–HREEs, calculated from the average REEs of Miocene zircon rims and each of the analysed points on the "GARBIG" traverse (shown as *shaded lines* without symbols except for the curve calculated from the garnet rim composition which is highlighted by *solid circles*). Shown for comparison are values of $^{REE}D_{zir/gt}$ presented by Rubatto (2002) from two unzoned garnets in the Reynolds Range, Australia, and a zoned garnet from Sesia Lanzo (see text for further details)

values of Rubatto (2002) is obtained for zircon forming in equilibrium with the garnet rim, entirely consistent with our petrographic observations. Rubatto (2002) suggested that differences between the estimated granulite $^{REE}D_{zir/gt}$ values and those calculated from the eclogite data may result from differences in pressure and/or temperature. Our data (Fig. 10) show slightly different estimated $^{REE}D_{zir/gt}$ values across the MREEs–HREEs from those of the Sesia-Lanzo eclogitic zircons, which may also reflect different garnet major-element compositions between the two studies. We suggest that the $^{REE}D_{zir/gt}$ values of Rubatto (2002) may reasonably be applied to other studies of zircon growth in metamorphic environments, although some caution over precise quantitative application should be applied until the dependence of these values on pressure, temperature and garnet composition has been fully evaluated.

Conclusions

Combined SIMS U–Th–Pb and REE data, petrographic and cathodoluminescence imaging analysis of zircon and garnet in a garnet granulite from the Carractraca peridotite body in the western Betic Cordillera suggest the following.

1. CL imaging reveals identical morphologies and internal structures for zircon grains hosted in the rim regions of garnet and those in the matrix; specifically, thick, CL-homogeneous, structureless rims occur in both environments, implying that this phase crystallised either before or during growth of the garnet rims.
2. U–Pb analyses of CL-homogeneous rims in zircon grains separated from garnet are indistinguishable from those reported by Platt and Whitehouse (1999) for zircon grains from the whole rock; these two data sets yield a refined age of 21.3 ± 0.3 Ma (2σ) for crystallisation of this phase of zircon.
3. REE analyses reveal that the thick, CL-homogeneous rims are strongly depleted in HREEs relative to their (presumed) igneous cores. The presence of large amounts ($< 25\%$ by volume) of modal garnet is suggested as a mechanism for depleting the rock of HREEs prior to, or during zircon rim growth. Together with the petrographic evidence ruling out pre-zircon garnet growth (conclusion 1 above), this constrains zircon growth to being essentially synchronous with the growth of garnet.
4. Aluminosilicate inclusions in the garnet record growth under conditions of decreasing pressure and increasing grossular content and are consistent with the initiation of partial melting during this decompression. We propose that the contemporaneously formed, 21.3 ± 0.3 Ma zircon rims record a point on the decompression path of PB383, rather than peak metamorphic conditions. Continued growth of garnet suggests that temperature was still rising at this stage of decompression.
5. MREE enrichments in some of the CL-homogeneous zircon rims relative to the core suggest either transport of REEs to the site of crystallisation/recrystallisation or localised dissolution followed by re-precipitation of an originally heterogenous zircon. At least partial operation of the latter mechanism is suggested by replication of atypical non-chondritic Y/Ho and Zr/Hf ratios in the rim and core of one of the analysed grains.
6. Garnet REE analyses show marked depletion of HREEs (as well as slight enrichments of LREEs–MREEs) towards the more Fe,Mn-rich rim; this may also be attributed to the large amount of modal garnet progressively depleting the rock of HREEs. The MREE enrichment probably results from more favourable substitution of larger ions into garnet as decompression continues.

Acknowledgements We thank John Hanchar and Nigel Kelly for thorough and constructive reviews. The Nordsim ion-microprobe facility in Stockholm is funded by the natural science funding agencies of Denmark, Finland, Norway and Sweden, and the Swedish Museum of Natural History. M.J.W. acknowledges the support of a senior research fellowship from Vetenskapsrådet, Sweden. Work by J.P.P. was funded by grant number GR3/13160 from the Natural Environmental Research Council of Great Britain. This is Nordsim laboratory contribution number 65.

References

Anders E, Grevesse N (1989) Abundances of the elements: meteoritic and solar. Geochim Cosmochim Acta 53:197–214

Argles TW, Platt JP, Waters DJ (1999) Attenuation and excision of a crustal section during extensional exhumation: the Carratraca Massif, Betic Cordillera, Southern Spain. J Geol Soc Lond 156:149–162

Balanyá JC, Azañon JM, Sánchez-Gómez M, García-Dueñas V (1993) Pervasive ductile extension, isothermal decompression, and thinning of the Jubrique unit in the Palaeogene (Alpujarride Complex, western Betics Spain). CR Acad Sci Paris 316:1595–1601

Barbey P, Allé P, Brouand M, Albarède F (1995) Rare-earth patterns in zircons from the Manaslu granite and Tibetan Slab migmatites (Himalaya): insights in the origin and evolution of a crustally-derived granite magma. Chem Geol 125:1–17

Bau M (1996) Controls on the fractionation of isovalent trace elements in magmatic and aqueous systems; evidence from Y/ Ho, Zr/ Hf, and lanthanide tetrad effect. Contrib Mineral Petrol 123:323–333

Bea F, Montero P (1999) Behavior of accessory phases and redistribution of Zr, REE, Y, Th, and U during metamorphism and partial melting of metapelites in the lower crust: an example from the Kinzigite Formation of Ivrea-Verbano, NW Italy. Geochim Cosmochim Acta 63:1133–1153

Bea F, Montero P, Garuti G, Zacharini F (1997) Pressure-dependence of rare earth element distribution in amphibolite- and granulite-grade garnets. A LA-ICP-MS study. Geostand Newslett 21:253–270

Bingen B, Austhreim H, Whitehouse M (2001) Ilmenite as a source for zirconium during high-grade metamorphism? textural evidence from the Caledonides of W. Norway and implications for zircon geochronology. J Petrol 42:355–375

Bouybaouène M, Michard A, Goffé B (1998) High-pressure granulites on top of the Beni Bousera peridotites, Rif belt, Morocco: a record of an ancient thickened crust in the Alboran domain. Bull Soc Géol Fr 169:153–162

Fraser G, Ellis D, Eggins S (1997) Zirconium abundance in granulite-facies minerals, with implications for zircon geochronology in high-grade rocks. Geology 25:607–610

Garbe-Schönberg CD, Arpe T (1997) High resolution-ICPMS in fast scanning mode: application for laser ablation analysis of zircon. Fresenius J Anal Chem 359:462–464

Hinton RW (1990) Ion microprobe trace-element analysis of silicates: measurement of multi-element glasses. Chem Geol 83:11–25

Hinton RW, Upton BGJ (1991) The chemistry of zircon; variations within and between large crystals from syenite and alkali basalt xenoliths. Geochim Cosmochim Acta 55:3287–3302

Hoskin PWO (1998) Minor and trace element analysis of natural zircon (ZrSiO4) by SIMS and laser ablation ICPMS: a consideration and comparison of two broadly competitive techniques. J Trace Microprobe Tech 16:301–326

Kornprobst J (1969) Le massif ultrabasique des Beni Bouchera (Rif Interne, Maroc): étude des péridotites de haute température et de haute pression, et des pyroxénolites, grenat ou sans grenat, qui leur sont associées. Contrib Mineral Petrol 23:283–322

Loomis TP (1972a) Contact metamorphism of pelitic rock by the Ronda ultramafic intrusion, southern Spain. Geol Soc Am Bull 83:2449–2474

Loomis TP (1972b) Diapiric emplacement of the Ronda high-temperature ultramafic intrusion, southern Spain. Geol Soc Am Bull 83:2475–2496

Monié P, Torres-Roldán R-L, García-Casco A (1994) Cooling and exhumation of the western Betic Cordilleras, 40Ar/ 39Ar thermochronological constraints on a collapsed terrane. Tectonophysics 238:353–379

Montel JM, Kornprobst J, Vielzeuf D, Veschambre M (1995) Shielding effect of garnet for the U-Th-Pb system in monazite: an e-probe study at Beni Bousera (Morocco). Terra Abstr 8:348

Nesbitt RW, Hirata T, Butler IB, Milton JA (1997) UV laser ablation ICP-MS; some applications in the earth sciences. Geostand Newslett 21:231–243

Pearce NJG, Perkins WT, Westgate JA, Gorton MP, Jackson SE, Neal CR, Chenery SP (1996) A compilation of new and published major and trace element data for NIST SRM 610 and NIST SRM 612 glass reference materials. Geostand Newslett 21:115–144

Platt JP, Vissers RLM (1989) Extensional collapse of thickened continental lithosphere: a working hypothesis for the Alboran Sea and the Gibraltar arc. Geology 17:540–543

Platt JP, Whitehouse MJ (1999) Early Miocene high-temperature metamorphism and rapid exhumation in the Betic Cordillera (Spain): evidence from U-Pb zircon ages. Earth Planet Sci Lett 171:591–605

Roberts MP, Finger F (1997) Do U-Pb zircon ages from granulites reflect peak metamorphic conditions? Geology 25:319–322

Rubatto D (2002) Zircon trace element geochemistry: partitioning with garnet and the link between U-Pb ages and metamorphism. Chem Geol 184:123–138

Sánchez-Rodriguez L (1998) Pre-Alpine and alpine evolution of the Ronda ultramafic complex and its country-rocks (Betic chain, southern Spain): U-Pb SHRIMP zircon and fission-track dating. PhD Thesis, Swiss Federal Institute of Technology, Zürich

Sánchez-Rodriguez L, Gebauer D (2000) Mesozoic formation of pyroxenites and gabbros in the Ronda area (southern Spain), followed by Early Miocene subduction metamorphism and emplacement into the middle crust: U-Pb sensitive high-resolution ion microprobe dating of zircon. Tectonophysics 316:19–44

Schaltegger U, Fanning CM, Guenther D, Maurin JC, Schulmann K, Gebauer D (1999) Growth, annealing and recrystallization of zircon and preservation of monazite in high-grade metamorphism; conventional and in-situ U-Pb isotope, cathodoluminescence and microchemical evidence. Contrib Mineral Petrol 134:186–201

Schreiber HD, Lauer HV, Thanyasiri T (1980) The redox state of cerium in basaltic magmas: an experimental study of iron-cerium interactions in silicate melts. Geochim Cosmochim Acta 44:1599–1612

Sosson M, Morillon AC, Bourgois J, Feraud G, Poupeau G, Saint-Marc P (1998) Late exhumation stages of the Alpujarride Complex (western Betic Cordilleras, Spain); new thermochronological and structural data on Los Reales and Ojen nappes. Tectonophysics 285:253–273

Spear FS, Kohn MJ (1996) Trace element zoning in garnet as a monitor of crustal melting. Geology 24:1099–1102

Stacey JS, Kramers JD (1975) Approximation of terrestrial lead isotope evolution by a two-stage model. Earth Planet Sci Lett 26:207–221

Steiger RH, Jäger E (1977) Subcommission on geochronology; convention on the use of decay constants in geo- and cosmochronology. Earth Planet Sci Lett 36:359–362

Torres-Roldán RL (1981) Plurifacial metamorphic evolution of the Sierra Bermeja peridotite aureole (Southern Spain). Estudios Geol 37:115–133

Tubía JM, Navarro-Vila F, Cuevas J (1993) The Maláguide–Los Reales Nappe: an example of crustal thinning related to the emplacement of the Ronda peridotites (Betic Cordillera). Phys Earth Planet Interiors 78:343–354

Vavra G, Schmid R, Gebauer D (1999) Internal morphology, habit and U-Th-Pb microanalysis of amphibolite-to-granulite facies zircons: geochronology of the Ivrea Zone (Southern Alps). Contrib Mineral Petrol 134:380–404

Vissers RLM, Platt JP, van der Wal D (1995) Late orogenic extension of the Betic Cordillera and the Alboran Domain: a lithospheric view. Tectonics 14:786–803

Whitehouse MJ, Claesson S, Sunde T, Vestin J (1997) Ion-microprobe U–Pb zircon geochronology and correlation of Archaean gneisses from the Lewisian Complex of Gruinard Bay, north-west Scotland. Geochim Cosmochim Acta 61:4429–4438

Whitehouse MJ, Kamber B, Moorbath S (1999) Age significance of U-Th-Pb zircon data from early Archaean rocks of west Greenland—a reassessment based on combined ion-microprobe and imaging studies. Chem Geol 160:201–224

Wiedenbeck M, Allé P, Corfu F, Griffin WL, Meier M, Oberli F, von Quadt A, Roddick JC, Spiegel W (1995) Three natural zircon standards for U-Th-Pb, Lu-Hf, trace element and REE analysis. Geostand Newslett 19:1–23

Zeck HP, Whitehouse MJ (1999) Hercynian, Pan-African, Proterozoic and Archean ion-microprobe zircon ages for a Betic-Rif core complex, Alpine Belt, W. Mediterranean—consequences for its P-T-t path. Contrib Mineral Petrol 134:134–149

Zeck HP, Monié P, Villa IM, Hansen BT (1992) Very high rates of cooling and uplift in the Alpine belt of the Betic Cordilleras, southern Spain. Geology 20:79–82